The structure and magnetic moment distribution in the antiferromagnetic phase of $U_{14}Au_{51}$

1997 J. Phys.: Condens. Matter 9 4729

(http://iopscience.iop.org/0953-8984/9/22/023)

J. Phys.: Condens. Matter **9** (1997) 4729–4742. Printed in the UK PII: S0953-8984(97)81722-5

The structure and magnetic moment distribution in the antiferromagnetic phase of $U_{14}Au_{51}$

P J Brown†‡, J Crangle§, K-U Neumann‡, J G Smith‡ and K R A Ziebeck‡

† Institut Laue Langevin, BP 156, 38042 Grenoble Cédex, France

‡ Department of Physics, Loughborough University, Loughborough, Leicestershire, LE11 3TU, UK

§ Department of Physics, University of Sheffield, S3 7RH, UK

Received 10 February 1997

Abstract. The antiferromagnetic structure of the intermetallic compound $U_{14}Au_{51}$ has been determined from neutron polarimetric measurements and refined by combining these data with integrated intensity measurements. The structure was found to be non-collinear with the U moments confined to the ***a*–*b*** plane. The moments of U atoms in each of the two sets of sixfold sites are arranged hexagonally with rotations of 60° between them and the two sets are rotated with respect to one another by 50°. The third (twofold) set of U atoms has no ordered moment. These conclusions are in disagreement with a previous determination of the structure from powder data which gave a collinear structure with moments parallel to the *c* axis. Magnetization measurements made on single crystals in the temperature range 300–2 K can be understood in terms of a transition to a non-collinear easy plane antiferromagnetic structure stable below 22 K. Polarized neutron measurements have been used to determine the contribution of each of the U sites to the susceptibility between 22 and 2 K. These show that of the two sixfold U sites, that with the smaller ordered moment contributes more than half of the total susceptibility. The twofold site, which is characterized by a small U–U separation, makes the smallest contribution.

1. Introduction

There has been considerable interest in recent years in the magnetic behaviour of actinide atoms in metallic systems [1, 2]. In actinides, as opposed to rare earth systems, the f electrons which carry the magnetism can participate in the Fermi surface and this leads to varied and complex electronic properties including heavy-fermion behaviour, superconductivity and antiferromagnetism. The present investigation is part of an ongoing study of the f–d interactions in U atoms in different metallic environments through the effects that they have on the stability of the magnetic moment, and on its spatial distribution. This study of the compound $U_{14}Au_{51}$ was motivated by the combination of interesting properties it displays. The magnetic susceptibility suggests antiferromagnetic order at temperatures below 22 K [3] and at the present time examples of antiferromagnetic metallic compounds in which uranium is the only magnetic species are rare. It has also been classified as a heavy-fermion system [4]. The γ value $\gamma(0) \simeq 300$ mJ K^{-2} (mol U)$^{-1}$ is five times greater than the value $\gamma(0) \simeq 60$ mJ K^{-2} (mol Ce)$^{-1}$ found in the isostructural compound $Ce_{14}Au_{51}$ [5]. The fact that there are three crystallographically distinct U sites in the $U_{14}Au_{51}$ structure makes it particularly interesting; differences in their behaviour can be used to help to clarify the influence of local environment on the behaviour of f electrons within the same structure.

0953-8984/97/224729+14$19.50

2. Previous work

The intermetallic compound $U_{14}Au_{51}$ crystallizes in the hexagonal $Gd_{14}Ag_{51}$ structure with space group $P6/m$ [6]. The uranium atoms occupy three crystallographically distinct sites 6(k), 6(j) and 2(e) labelled U1, U2 and U3 respectively. The crystallographic parameters of the structure are given in table 1. The structure can be visualized by considering first the arrangement of the three types of U atom. The network formed by the U2 atoms which lie in the $z = 0$ plane is shown in figure 1(a). The shortest bonds in this plane (4.415 Å) link the U2 atoms in hexagons centred at (000) and are shown as solid lines. These hexagons are linked to one another by the next-nearest-neighbour bonds (4.843 Å) shown as dashed lines. The U1 atoms lie in a similar layer at $z = \frac{1}{2}$, but in this case the nearest-neighbour bonds (4.109 Å) are between U2 atoms belonging to different hexagons, and the next-nearest-neighbour bonds (4.308 Å) form triangles as shown in figure 1(b). The two remaining U atoms (U3) lie on the hexad axis at $z = \pm 0.3$. Each is closely linked to just one U3 neighbour across the plane at $z = \frac{1}{2}$. The gold atoms in the (j) and (k) positions fill the spaces within the U layers and the remaining gold atoms serve to separate them as shown in figure 2.

Table 1. Crystallographic data for the structure of $U_{14}Au_{51}$.

Space group $P6/m$	$Z = 1$	Type	$Gd_{14}Ag_{51}$				
Cell dimensions (Å)	$a = 12.652$	$c = 9.138$					
Atom positions:		from [3]			this study		
		x	y	z	x	y	z
6 U1 in 6(k)	$(x, y, \frac{1}{2})$	0.138(2)	0.463(2)		0.142(2)	0.463(1)	
6 U2 in 6(j)	$(x, y, 0)$	0.398(2)	0.109(2)		0.391(1)	0.114(1)	
2 U3 in 2(e)	$(0, 0, z)$			0.304(3)			0.304(2)
12 Au1 in 12(l)	(x, y, z)	0.073(1)	0.265(1)	0.240(1)	0.0792(10)	0.2680(9)	0.2319(8)
12 Au2 in 12(l)	(x, y, z)	0.116(1)	0.494(1)	0.146(2)	0.116(1)	0.4944(1)	0.153(1)
12 Au3 in 12(l)	(x, y, z)	0.443(1)	0.102(1)	0.336(2)	0.443(1)	0.103(1)	0.3343(8)
6 Au4 in 6(k)	$(x, y, \frac{1}{2})$	0.231(2)	0.049(2)		0.237(1)	0.058(1)	
3 Au5 in 6(j)	$(x, y, 0)$	−0.022(4)	0.101(4)		−0.136(3)	−0.027(6)	
4 Au6 in 4(h))	$(\frac{1}{3}, \frac{2}{3}, z)$			0.311(3)			0.310(1)
2 Au7 in 2(c)	$(\frac{1}{3}, \frac{2}{3}, \frac{1}{4})$						

Susceptibility, specific heat and resistivity indicate a magnetic phase transition at 22 K [3]. This has been confirmed by neutron powder diffraction measurements: an antiferromagnetic structure with zero propagation vector and magnetic space group $P6'/m$ was proposed [7]. The ordered magnetic moments aligned parallel to $\boldsymbol{c}$ were 0.5 and $1.6\mu_B$ on the U atoms in the 6(k) (U1) and 6(j) (U2) positions respectively. No moment was assigned to the U3 atoms on the 2(e) sites. These atoms have a particularly small separation and it is argued that direct f-electron wave-function overlap prevents a magnetic response.

3. Material

A single crystal of $U_{14}Au_{51}$ weighing about 30 g was grown by the Czochralski method from spectroscopically pure uranium and gold melted together in the appropriate proportions. All

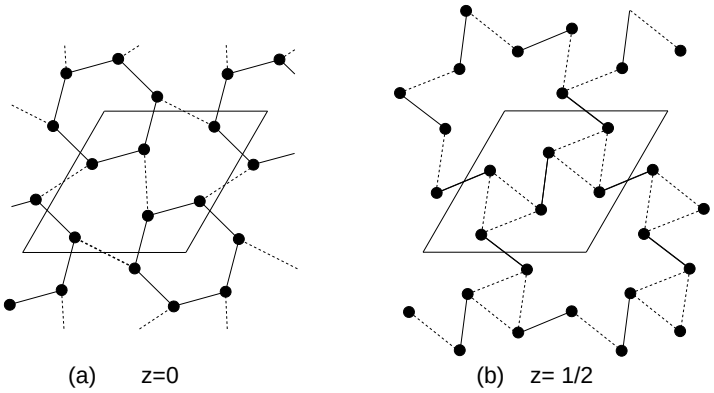

Figure 1. The networks of U atoms in the planes perpendicular to c at (a) $z = 0$ the U2 plane, and (b) $z = 1/2$ the U1 plane, of $U_{14}Au_{51}$. In each plane the shortest U–U vectors are shown as solid and the next shortest as dashed lines.

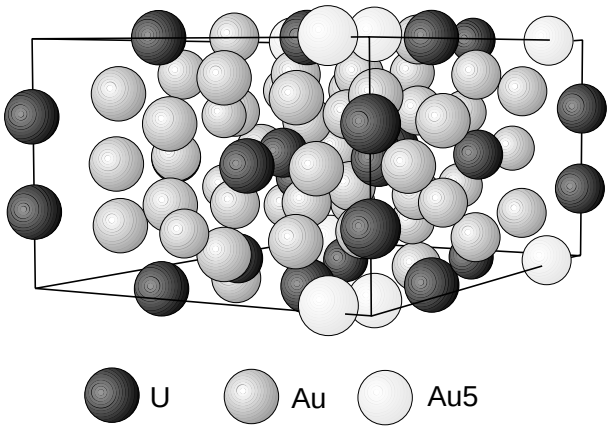

Figure 2. Schematic representation of the structure of $U_{14}Au_{51}$. The Au5 sites, shown as light-grey spheres, are only half occupied.

the specimens used for the work described in this paper were single crystals cut from this boule.

4. Magnetization measurements

In an earlier communication the results of exploratory magnetization measurements on two $U_{14}Au_{51}$ single crystals samples were reported [8]. These same samples were used in the present, more detailed, study; they had dimensions about $4 \times 2 \times 2\times$ mm^3 with their long axes aligned respectively within a few degrees of the [001] (c) and [010] (b) crystallographic axes. The magnetization measurements were made on a SQUID magnetometer in which the field could be varied from -5T to $+5$T and the temperature from 295 K to 2 K. The new measurements were made at much more closely spaced temperature intervals than those reported earlier. It was found that in both samples and at all temperatures the susceptibility was almost independent of field. The small temperature dependence was corrected by the method introduced by Arrott [9] from plots, for each specimen at each temperature, of the

square of the magnetization against the ratio of field to magnetization. The correction from the measured values was never more that a few parts per thousand even at the highest field (5.0 T). The variation of the susceptibility with temperature for both samples is shown in figure 3. As in the previous measurements a maximum in the susceptibility occurs around 22 K which is ascribed to the antiferromagnetic transition. At temperatures above the susceptibility maximum the reciprocal susceptibility follows a linear Curie–Weiss law, but the lines corresponding to different crystallographic directions are quite distinct. The values derived for the effective moments (p_{eff}) and the paramagnetic Curie temperatures (Θ_p) are shown in table 2. The effective moment given is an average over all the U atoms in the unit cell; its value for the two field directions is not significantly different. Θ_p on the other hand shows very definite anisotropy. Below the antiferromagnetic Néel temperature T_N the temperature dependence of the susceptibility is even more strongly anisotropic. The $\boldsymbol{c}$-axis susceptibility varies very little around T_N which is not consistent with the moments being parallel to $\boldsymbol{c}$ in the antiferromagnetic phase. The $\boldsymbol{b}$-axis susceptibility has a maximum at T_N then drops to a minimum at around 8 K after which it begins to rise again slightly. It was originally thought, erroneously, that this minimum might be indicative of a further phase change. The observation that neither the parallel or perpendicular susceptibilities tends to zero at low temperatures suggests that the low-temperature magnetic structure may be non-collinear.

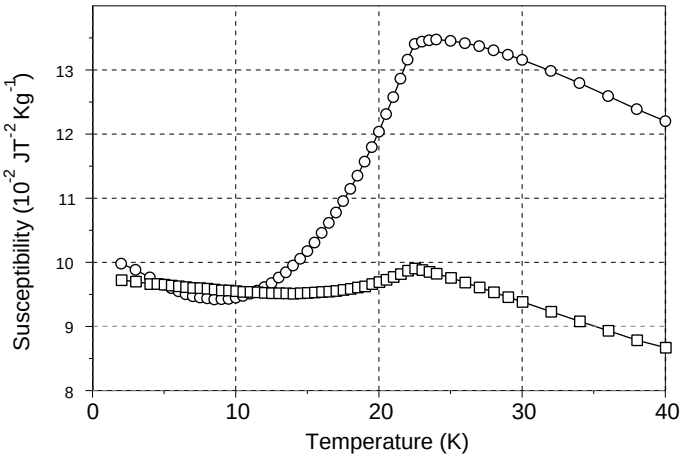

Figure 3. Temperature dependence of the magnetic susceptibility of a single crystal of $U_{14}Au_{51}$ between 2 K and 30 K. □ and ○ are for fields parallel and perpendicular to $\boldsymbol{c}$ respectively.

Table 2. The effective moments, paramagnetic Curie temperatures and Néel temperatures obtained from magnetic susceptibility measurements on $U_{14}Au_{51}$.

Field direction	Θ_p (K)	p_{eff} (μ_B/U)	T_N (K)
$\boldsymbol{b}$ axis	− 71(1)	3.19(5)	22.0(2)
$\boldsymbol{c}$ axis	−111(1)	3.12(5)	21.3(2)

5. Neutron scattering measurements

Neutron scattering measurements were made on a small single crystal of $U_{14}Au_{51}$ ($6 \times 2 \times 1$ mm^3) cut from the same boule as that used for the magnetization measurements. The long axis of the crystal was some 8° off the $\boldsymbol{c}$ axis.

5.1. Integrated intensities

Integrated intensity measurements on this single crystal were made on the four-circle diffractometer D10 at ILL. The initial object of the experiment was to investigate the origin of the observed upturn in the susceptibility at ∼8 K which had been observed in the magnetization measurements. The crystal was mounted in the four-circle He-flow cryostat developed for D10 [10]. Before cooling below the Néel temperature the integrated intensities of a set of reflections with $\sin\theta/\lambda < 0.5$ Å^{-1} were measured at 30 K to allow refinement of the nuclear structure at low temperature. Since the magnetic and nuclear scattering are superposed in this structure and in general the magnetic contribution to the intensity is much weaker than the nuclear one, a set of low-angle reflections was chosen for which the nuclear structure factors were relatively weak. The integrated intensities of this set were measured at 2 K, 4 K, 8 K, 12 K and 16 K. The contribution of magnetic scattering to these reflections was obtained by subtracting the intensity of the nuclear scattering measured at 30 K. The intensities of three reflections 010, 011 and 110 were followed as a function of temperature from 30 K to 2 K to confirm the phase transition at 22 K and to investigate the anomalous behaviour in the [110] direction reported by [7]. The integrated intensities of these three reflections are plotted against temperature in figure 4. All three show a smooth variation in intensity from a maximum at 2 K to a constant value due to nuclear scattering at 22 K. The anomalous behaviour of the 110 peak as a function of temperature reported by [7] was not observed in this experiment, nor was there any abrupt change in the magnetic intensities around 10 K which could have indicated a second phase transition.

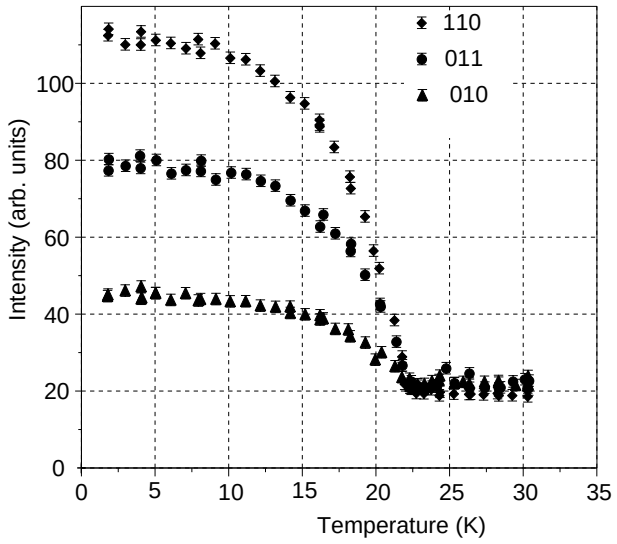

Figure 4. Temperature dependence of the integrated intensities of the 110, 011 and 010 reflections in $U_{14}Au_{51}$ between 32 and 5 K.

The integrated intensities measured at 30 K were corrected for absorption and used in a structure refinement for the positional parameters. The thermal parameters were fixed at low values since the measured data set was limited to $\sin\theta/\lambda < 0.5$ Å^{-1}. There was good agreement between the parameters obtained in the refinement, reported in table 1, and those of the published nuclear structure at 30 K [7]. The intensities of magnetic scattering obtained from the differences in integrated intensities measured at 12 and 30 K are given in table 3. They have been converted to barns by comparison with the nuclear scattering. The magnetic intensities calculated for the structure proposed by [7] are given for comparison. It is apparent that the previously reported magnetic structure is not compatible with our measurements of the magnetic scattering although our measured intensities do agree substantially with those deduced in the powder work. It is clear that the disagreement between the observed and calculated powder patterns is due to an inadequate model for the structure rather than to systematic errors in the powder data. Since the use of a single crystal allows many more magnetic reflections to be measured the disagreement is much more marked in the present study.

Table 3. Observed and calculated magnetic cross-sections for $U_{14}Au_{51}$ at 12 K. $F^2_{calc}(1)$ is for the structure of [3] and $F^2_{calc}(2)$ for the structure proposed in this paper.

h	k	ℓ	F^2_{obs}	σF^2_{obs}	$F^2_{calc}(1)$	$F^2_{calc}(2)$
0	1	0	0.8767	0.0632	0.2047	1.0226
1	1	0	3.6606	0.1199	2.6594	4.0748
2	1	0	1.6213	0.0980	0.1612	1.5287
3	1	0	0.4188	0.2218	0.0856	0.1238
0	2	0	2.9185	0.1129	1.1168	2.5899
1	2	0	0.2273	0.0398	0.2148	0.2658
2	2	0	0.0000	0.0000	0.1815	0.0134
1	3	0	0.0000	0.0000	2.0591	0.0078
0	0	1	0.0000	0.0000	0.0000	0.0000
0	1	1	2.2276	0.0986	0.5407	2.4969
1	1	1	0.8777	0.0740	0.6375	1.0393
2	1	1	0.1437	0.0277	0.1507	0.0616
0	2	1	1.8789	0.1336	1.1918	1.7297
1	2	1	0.5684	0.0723	0.1718	0.3879
0	3	1	0.1644	0.0356	0.3014	0.0556
0	0	2	0.0000	0.0000	0.0000	0.0000
0	1	2	0.8333	0.0513	0.0198	0.6931
1	1	2	3.2111	0.1571	0.6027	2.9583
2	1	2	1.1047	1.2357	0.0594	1.2489
0	2	2	2.4292	0.2921	0.3022	1.7428
1	2	2	0.4507	0.1490	0.0782	0.3014

5.2. Polarized neutron flipping ratios

Measurements of the polarization dependence of the intensities of the Bragg reflections of a magnetized crystal can give unique information about spatial distribution of the electrons which contribute to the susceptibility. This is particularly useful in materials such as $U_{14}Au_{51}$ in which there are several crystallographically distinct sites which may contribute to the magnetization and it is for this reason that measurements of polarized neutron flipping ratios have been made.

The $U_{14}Au_{51}$ crystal was mounted with its long axis vertical on the polarized neutron diffractometer D3 at ILL inside the variable-temperature chamber of a superconducting magnet. A vertical field of 4.6 T was applied to magnetise the crystal. Since the unit cell is quite large and the expected magnetic signal quite small it was not possible to attempt to measure a complete set of even just the $hk0$ reflections in the time available. To limit the number of measurements reflections were selected which obeyed the following criteria. (i) A nuclear structure factor greater than 2×10^{-12} cm. (ii) A geometric structure factor of 1 or greater for at least one of the three different U atoms. (iii) A large algebraic difference between the geometric structure factors for at least two out of the three. A set of 34 inequivalent $hk0$ and 3 $hk1$ reflections with $\sin\theta/\lambda < 0.4$ Å^{-1} were selected using these criteria. For each of these reflections three members of the form were chosen and their flipping ratios measured at a temperature of 14 K. Further measurements of a set of reflections, reduced by omitting those for which very little magnetic scattering had been observed at 14 K, were made at 2 K and just above the Néel transition, at 22 K.

The flipping ratios were converted to magnetic structure factors in the usual way, introducing the correction for lack of perfect polarization and using the the structural parameters obtained in section 5.1 to calculate the necessary nuclear structure factors. The values obtained for equivalent reflections were averaged and the standard deviation of the magnetic structure factors estimated from the deviations of individual values from the mean. In no case were these standard deviations significantly different from those estimated from the counting statistics. The contributions to the magnetic scattering from the diamagnetism of the core electrons [11] and from Schwinger scattering [12] have been subtracted from the measured data: these corrections were of the same order or less than the standard deviations.

The magnetic structure factors were used in a least-squares procedure to determine the moments induced by the applied field on the three independent U sites of the structure. Since the ratio of spin to orbital moment is not known *a priori* in a metallic compound [13] this ratio was left as a free variable. In the dipole approximation the uranium magnetic form factor can be written $f_U = \langle j_0\rangle + C_2\langle j_2\rangle$, where the coefficient $C_2 = \mu_L/(\mu_S + \mu_L)$ is the ratio between the orbital and the total moment of the U atom. The $\langle j_{0,2}\rangle$ functions are obtained from the radial density of the U 5f electrons calculated by Desclaux and Freeman [14]. The results of the initial least-squares fit of this model to the 14 K data were not very satisfactory; the goodness of fit measured by $\chi^2 = \sum_{obs}\left((F_{obs} - F_{calc})/\sigma^2\right)/(n_{obs} - n_{pars})$ was $\sim$5 suggesting that the simple spherical model was not adequate. The fitted parameters are reported in table 4; there was a high correlation between μ_L and μ_S for all the sites.

In order to see in what way the model was unable to fit the data a Fourier projection down [001] was made in which the Fourier coefficients were the differences, $F_{obs} - F_{calc}$, between the measured structure factors and those calculated for the fitted model obtained above. The map was constructed using the method of maximum entropy so that the resulting map is the flattest one which is consistent with the data, taking into account its variance [15]. It is shown in figure 5. Because the set of $hk0$ data is far from complete not much significance should be given to the details of the map, but the major features are significant peaks of positive and negative density close to and on either side of the U2 sites. This gives a strong indication that the peak of the magnetization induced by the applied field is not centred on the atom but displaced from it in the direction of positive gradient. The simple model was accordingly modified to allow the x and y parameters fixing the centres of the spherical magnetization distribution on U1 and U2 to vary. This immediately gave a much improved fit with the parameters given in the second column of table 4 and $\chi^2 \sim 1.5$. Of the positional parameters only x of U2 changes significantly.

For the model above the ratio of observations to parameters is rather low: 37/10 for the

Table 4. Parameters of the model used to fit the magnetization induced by a field of 4.6 T applied parallel to the $\boldsymbol{c}$ axis of $U_{14}Au_{51}$. The numbers in brackets are the standard deviations of the parameters; where none are given the parameters were fixed.

Parameter		14 K	14 K	14 K	22 K	2 K
U1	μ	0.026(23)	0.025(14)	0.038(3)	0.46(2)	0.034(2)
	C_2	3(2)	4(2)	2	2	2
	x	0.1421	0.142(3)	0.1421	0.1421	0.1421
	y	0.4651	0.458(4)	0.4651	0.4651	0.4651
U2	μ	0.103(23)	0.119(13)	0.102(10)	0.102(7)	0.121(6)
	C_2	2.1(5)	1.5(4)	2.1(2)	2.1(1)	1.5(2)
	x	0.3913	0.383(1)	0.383(1)	0.3810(7)	0.3822(8)
	y	0.1123	0.112(1)	0.113(1)	0.1089(9)	0.1106(8)
U3	μ	0.02(3)	0.02(1)	0.016(3)	0.012(2)	0.020(2)
	C_2	2(3)	2(2)	2	2	2
	χ^2	5	1.3	1.3	0.6	0.4

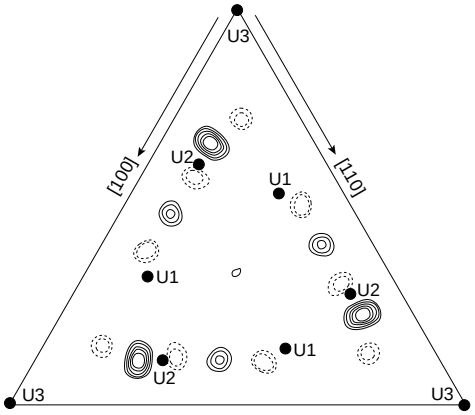

Figure 5. Maximum-entropy reconstruction of the magnetization distribution corresponding to the difference between the observed magnetic scattering and that calculated from the best fit to the simple model. The map shows the projection on (001). The projected positions of the U atoms are shown by ● .

14 K data and only 19/10 for the other two sets. It therefore seemed advisable to restrict the model somewhat, before fitting to these smaller data sets. Since the magnetization associated with the U1 and U3 sites is small it was decided to fix the constant C_2 to 2 for these two atoms. The value of 2 was chosen because it is within the range indicated by the general fit, close to that determined for U2 and consistent with the values determined for other U intermetallics [16]. Since there was no evidence that the centre of the magnetization on U1 is displaced from the centre of the atom, the U1 x and y were fixed to the atom coordinates. The model, now containing only six parameters, was fitted first to the 14 K data yielding $\chi^2 = 1.3$ and then to the 2 K and 22 K data giving $\chi^2 = 0.4$ and 0.6 respectively. The final parameters for each temperature are given in table 4.

5.3. Neutron polarimetry

The determination of the magnetic arrangement in structures with zero propagation vector is difficult because of the coincidence of the magnetic and nuclear reflections. This is particularly true for $U_{14}Au_{51}$ because for most of the reflections the magnetic scattering is at least an order of magnitude less than the nuclear scattering. As a consequence only a few of the magnetic structure factors can be determined with useful precision from integrated intensity measurements. Zero-field neutron polarimetry is a technique which is particularly applicable to the determination of structures with zero propagation vector [17]. It enables the ratio of the magnetic to nuclear scattering to be determined even if these are in quadrature, and gives direct information about the direction of the magnetic interaction vectors. Study of the depolarization of the scattered beams can also be used to determine the types of magnetic domain present and hence to deduce the magnetic space group [18]. For these reasons we have made some neutron polarimetric measurements on $U_{14}Au_{51}$ to obtain more direct structural information.

The polarimetry was carried out using the neutron polarimeter Cryopad II [19] installed on the sample table of the polarized neutron triple-axis spectrometer IN20 at ILL. The same single crystal of $U_{14}Au_{51}$ as was used in the previous experiments was mounted with its [010] axis vertical inside an ILL 'Orange' cryostat and placed within the annular zero-field chamber of Cryopad II. For each of a number of $h0\ell$ reflections with $\sin\theta/\lambda < 0.25$ the direction of the scattered polarization was determined with the incident polarization successively parallel to the vertical direction ($\boldsymbol{z}$), the scattering vector ($\boldsymbol{x}$) and the third direction ($\boldsymbol{y}$) which completes the right-handed Cartesian set. These axes are the 'polarization axes' and from their definition the magnetic interaction vector $\boldsymbol{Q}$ lies in the $\boldsymbol{y}$–$\boldsymbol{z}$ plane. The majority of the measurements were made with a wavelength of 1.53 Å and at a temperature of 15 K. To check the performance of the polarimeter and the possible influence of multiple scattering the 201 and 003 reflections were also measured at 25 and 20 K. Some further measurements at 15 K were made with a wavelength of 2.36 Å. The results obtained for the 200 and 201 reflections are illustrated in figure 6 by stereograms showing the input and scattered polarization directions and the magnitude of the scattered polarization. The most significant features of these results and the conclusions they impose are the following.

(i) For incident polarization ($\boldsymbol{P}$) parallel to the scattering vector ($\boldsymbol{x}$) the scattered beam is always depolarized to some extent. The direction of the scattered polarization is not rotated significantly and for the two reflections illustrated it is reversed. Such depolarization is due to the term $\mathrm{i}[\boldsymbol{P}\times\boldsymbol{Q}N^{*}-\boldsymbol{P}\times\boldsymbol{Q}^{*}N]$ in the expression for the scattered polarization [19]. It shows that the magnetic scattering is in quadrature with the nuclear scattering and that the crystal contains almost equal fractions of the two 180° domains. The reversal of the directions indicates that the magnetic structure factor is greater than the nuclear one for 200 and 201.

(ii) For the 200 reflection there is no significant rotation for any of the three input polarization directions, but appreciable depolarization occurs for incident polarization in the $\boldsymbol{x}$ and $\boldsymbol{y}$ but not in the $\boldsymbol{z}$ direction. The fact that there is no depolarization for the $\boldsymbol{z}$ direction means that the term in $\boldsymbol{P}\times\boldsymbol{Q}$ is zero for $\boldsymbol{P}$ parallel to z i.e. $\boldsymbol{Q}$ must be parallel to $\boldsymbol{z}$ (crystallographic [010]) for this reflection. There must therefore be components of moment in the $\boldsymbol{a}$–$\boldsymbol{b}$ plane and no significant component of the magnetic structure factor parallel to $\boldsymbol{c}$.

(iii) For 201 there is some depolarization for all three incident polarization directions and rotation of the polarization direction in the $\boldsymbol{x}$–$\boldsymbol{z}$ plane is observed. This is consistent with

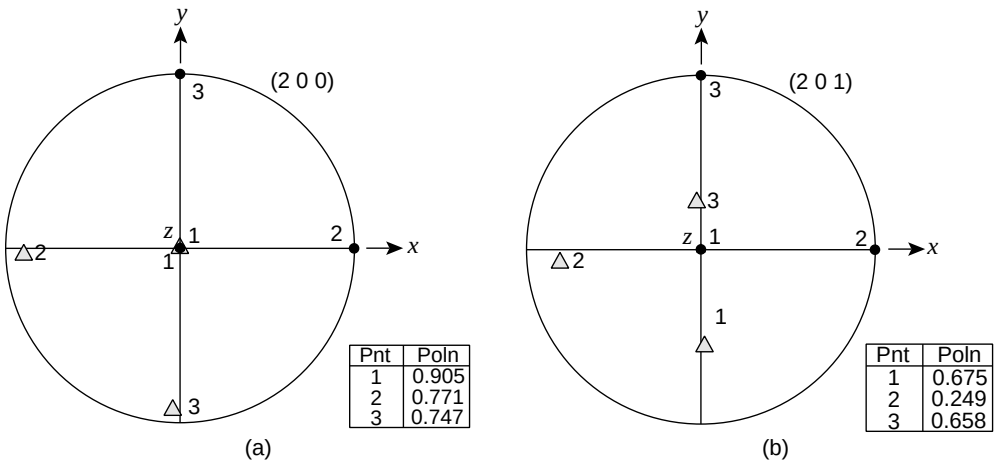

Figure 6. Stereograms showing the directions of incident and scattered polarizations for the 200 and 201 reflections of $U_{14}Au_{51}$ at 15 K. The symbols ● mark the incident polarization directions; the scattered polarization directions are marked △ and are all in the upper hemisphere. The numbers serve to identify corresponding pairs of directions and the magnitude of the scattered polarization. The stereograms are drawn with respect to the 'polarization axes'.

moments in the $\boldsymbol{a}$–$\boldsymbol{b}$ plane. The observation that the depolarization for incident directions in the $\boldsymbol{y}$–$\boldsymbol{z}$ plane, which is that containing the magnetic interaction vector, is less than for the $\boldsymbol{x}$ direction suggests that all the depolarization is due to the 180° domains and that there is none due to orientation domains. The magnetic structure must therefore have the full symmetry of the crystallographic space group.

6. Determination of the magnetic structure

The observations of the previous section put very severe constraints on possible models for the antiferromagnetic structure of $U_{14}Au_{51}$. In fact there is just a single magnetic space group and basic model structure which is compatible with all of them. It is shown by (ii) and (iii) above that the magnetic moments lie in the $\boldsymbol{a}$–$\boldsymbol{b}$ plane and the hexagonal symmetry is maintained. The U1 and U2 sites are on the mirror planes perpendicular to the hexad and their moments lie in it. These mirror planes cannot therefore invert the moments and hence are combined with time reversal. To satisfy (i) which implies that centro-symmetrically related atoms have opposite moments the hexad must operate without time inversion. The magnetic space group is therefore $P6/m'$ and the magnetic moments on the groups of six U1 (and U2) atoms related by the hexad have a 'star' structure as illustrated in figure 7. In this magnetic group any moment on the U3 atoms which lie on the hexagonal axes is constrained to be parallel to $\boldsymbol{c}$. The measurements show that this component of moment is small or zero. It is been assumed from here on that the U3 moment is zero, and no evidence has been found to contradict this assumption. To describe the structure completely it is necessary to determine the magnitude and the orientation within the $\boldsymbol{a}$–$\boldsymbol{b}$ plane of the moments on the U1 and U2 atoms. The polarimetric data for the 101 reflection which are given in table 5 were used to obtain rough values of the moment directions within the $\boldsymbol{a}$–$\boldsymbol{b}$ plane. The observation that incident polarization parallel to $\boldsymbol{y}$ is hardly changed on scattering by the 101 reflection shows that its magnetic interaction vector $\boldsymbol{Q}$ is nearly parallel to $\boldsymbol{y}$. The magnitude of $\boldsymbol{Q}$ can be obtained from the depolarization with incident

polarization parallel to $\boldsymbol{x}$

$$\frac{1-\gamma^2}{1+\gamma^2} = \frac{P_x}{P} \tag{1}$$

where $\gamma = |\boldsymbol{Q}|/|N|$ and N is the nuclear structure factor, giving $|\boldsymbol{Q}| \sim 0.76 \times 10^{-12}$ cm. The contributions to the magnetic interaction vector $\boldsymbol{Q}$ of the 101 reflection from the U1 and U2 moments were computed as a function of the angle ϕ between $\boldsymbol{a}^*$ ([210]) and the moment direction on the representative atom. The components Q_y and Q_z on the polarization axes are plotted in figure 8. The resultant magnetic interaction vector is obtained from the sum of the two, each with their own value of ϕ. It should be noted that the ϕ scales for U1 and U2 in figure 8 are displaced with respect to one another: the displacement has been chosen to demonstrate that there is a range of ϕs where the z components due to U1 and U2 cancel whilst the y components reinforce one another. Only one such region was found. It corresponds to ϕ U1 $\sim 140^\circ$, ϕ U2 $\sim 90^\circ$. A least-squares refinement of the magnetic structure was carried out in which the observations were the components of scattered polarization which had been measured in the experiment. These are compared to calculated values of the same components based on a model structure whose parameters are varied in the course of the refinement [20]. The refinement started with a model structure in which the U1 and U2 atoms had moments of 1 μ_B arranged as in figure 7 with angles ϕ U1 $= 140^\circ$, ϕ U2 $= 90^\circ$ as determined above. The refinement converged well, reducing the sum of squares by a factor of more than four in three cycles. The parameters obtained from the refinement are given in table 6. The final χ^2 of 90 is rather high but this is not unexpected as the standard deviations given to the observations were those due to counting statistics only. There are known to be other systematic errors, due to imperfect magnetic screening, which are particularly important when the scattered polarization is low. These are difficult to quantify. The low-angle reflections on which the polarimetric measurements were made were all rather weak, having nuclear structure factors of 1 or less compared with the maximum of 14. For such weak reflections the ratio of magnetic to nuclear scattering, and hence the moment values, obtained from polarimetry may be affected by multiple scattering. For this reason the moment values were also refined with a standard magnetic structure factor least-squares refinement program. The integrated intensities measured on D10 were used as data and the ϕ values were fixed to those obtained above. This refinement also converged well leading to a final χ^2 of 1.4 and moment values, reported in table 6, which were not significantly changed. This shows that the structure deduced from the polarimetric measurements is in excellent agreement with the integrated intensity measurements. In a final step the moment values obtained from the intensity refinement were used in a refinement of just the angles ϕ with the polarization components as data. These final values are also given in table 6, but again are not significantly changed. The structure corresponding to these parameters is illustrated in projection on (001) in figure 9. The calculated magnetic intensities are listed in the final column of table 3 where they may be compared with the experimental values.

7. Discussion

The polarimetric measurements show conclusively that the antiferromagnetic structure of $U_{14}Au_{51}$ is non-collinear with a triangular arrangement of moments lying in the $\boldsymbol{a}$–$\boldsymbol{b}$ plane. The symmetry does not constrain the moments to adopt symmetry directions in this plane, and there is a general angle between the moment directions on the uranium in the 6(j) and 6(k) sites. This rather complex structure is quite consistent with the observed

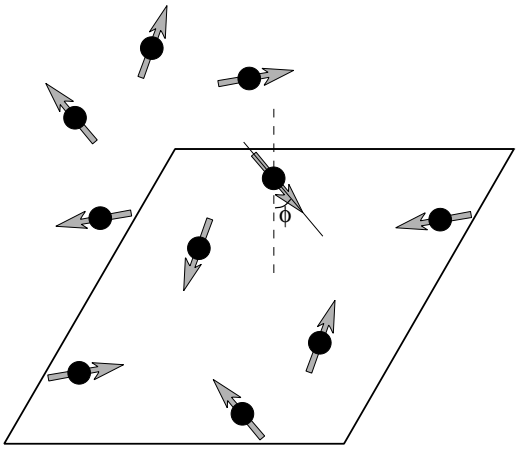

Figure 7. The hexagonal 'star' arrangement of moments found in the U1 and U2 layers of $U_{14}Au_{51}$. The angle ϕ used to fix the orientation of the U moments is marked.

Table 5. Polarization scattered by the 101 reflection of $U_{14}Au_{51}$ at 15 K for three incident polarization directions. The angles θ and ϕ are the spherical polar angles on the 'polarization axes'.

Incident polarization			Scattered polarization		
P	θ	ϕ	P	θ	ϕ
0.92	0	0	0.511(1)	175(1)	− 81(3)
0.92	90	0	0.502(1)	94(1)	−172(1)
0.92	90	90	0.910(1)	97(1)	95(1)

Table 6. Parameters of the magnetic structure of $U_{14}Au_{51}$. ϕ is the angle between $\boldsymbol{a}^*$ and the moment direction on the representative atom (table 1).

		Polarimetry only		Polarimetry with intensities
Atom	μ (μ_B)	ϕ(○)	μ (μ_B)	ϕ(○)
U1	2.10(7)	87.4(1.6)	2.28(6)	88.5(1.5)
U2	1.35(5)	140.2(2.3)	1.48(8)	138.7(2.1)

anisotropy in the magnetic susceptibility. In such a non-collinear structure none of the components of susceptibility is expected to fall to zero at low temperatures. This accords with the observations. Little temperature dependence of the $\boldsymbol{c}$-axis susceptibility is expected below T_N since there is no component of the antiferromagnetic moment parallel to $\boldsymbol{c}$. Understanding the temperature dependence of the $\boldsymbol{b}$-axis data is more difficult. The initial fall below T_N must arise because one-half of the antiferromagnetic moment is parallel to $\boldsymbol{b}$ so that its contribution to the susceptibility below T_N is small. The small anomalous variation at lower temperatures may be attributed to small changes in competing exchange interactions which change the relative orientations of the U1 and U2 planes of moment and hence their contributions to the susceptibility.

The exchange interactions can be divided into those between the U1 and U2

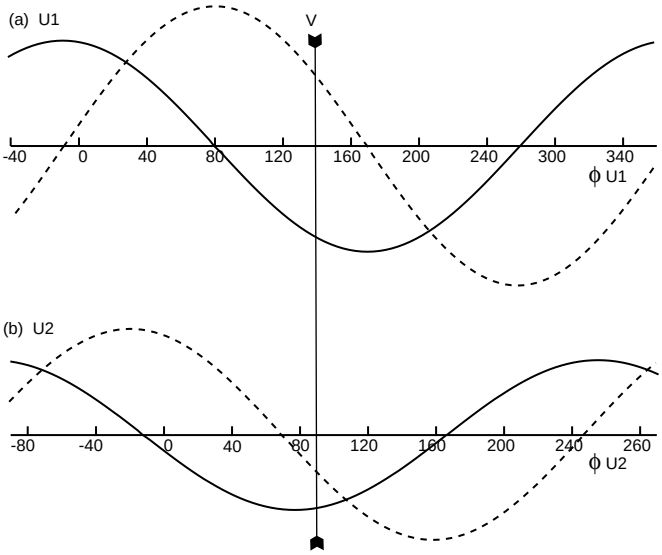

Figure 8. Curves showing the variation with ϕ of Q_y —— and Q_z - - - - components of the magnetic interaction vector of the 101 reflection of $U_{14}Au_{51}$. (a) is for the U1 atoms and (b) for the U2 atoms. The origins of the two figures are displaced so that on the vertical line marked V (ϕ (a) $= 140^\circ$, ϕ (b) $= 90^\circ$) the z components of U1 and U2 cancel whilst their y components reinforce one another.

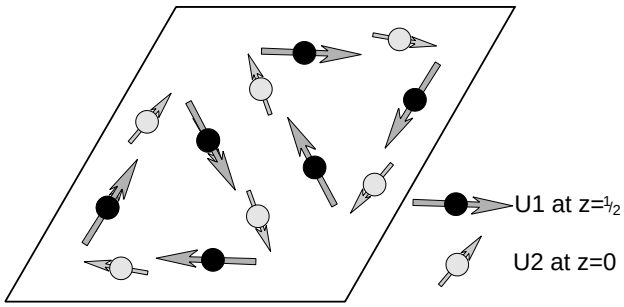

Figure 9. Projection on (001) of the magnetic structure of $U_{14}Au_{51}$ showing the relative orientations of the moments on the U1 and U2 atoms.

layers which are essentially ferromagnetic, and those within the layers which are primarily antiferromagnetic and largely frustrated. In the layer at $z = \frac{1}{2}$ (U1 atoms) an antiferromagnetic nearest-neighbour interaction can be satisfied but the triangular arrangement of next-nearest neighbours (figure 1(b)) leads to frustration of antiferromagnetic next-nearest-neighbour coupling. In the $z = 0$ layer (U2 atoms) the nearest and next-nearest distances are smaller; the larger ordered moment which was observed indicates stronger coupling, consistent with an RKKY interaction. The antiferromagnetic hexagonal symmetry ensures that the molecular field at the U3 sites due to U1 and U2 is zero, which explains why they have no ordered moment.

The polarized neutron scattering measurements show that the major part of the ***c***-axis susceptibility both in the antiferromagnetic phase and just above the Néel temperature is due to the U2 atoms which are those which have the smaller ordered moment. These atoms

contribute more than half the total susceptibility and their contribution is essentially the same at 22 K and 14 K. The total magnetization per cell due to U 5f electrons is 0.92(2), 0.88(2) and 0.89(2) μ_B at 22, 14 and 2 K respectively. The magnetizations in 4.6 T obtained from the squid measurements are 1.04(1), 1.02(1) and 1.06(1) μ_B per cell at the same temperatures. The difference suggests that there is a contribution to the magnetization of some 0.17 μ_B per cell from the 6d and conduction electrons. The fall in the susceptibility between 22 K and 14 K is due to a reduction in the susceptibility of the U2 site. This is not unexpected since this site carries the largest antiferromagnetic moment and is therefore presumably the most strongly antiferromagnetically coupled. The susceptibility of this site is smaller still at 2 K but the loss of magnetization is compensated by an apparent increase in the susceptibility of both the U1 and U3 sites between 22 and 2 K.

Perhaps the most surprising feature of the magnetization distribution is the displacement of the centre of the magnetization induced by a magnetic field parallel to the $\boldsymbol{c}$ axis from the centre of the atom determined in zero field. The direction of the displacement is essentially parallel to the direction of the antiferromagnetic moment. It may be due to an acentric component in the susceptibility of the U2 site, or to a displacement of the atomic centre under applied field. It is not possible to choose between these two possibilities with the data presently available, although they could be distinguished by carrying out a structure determination under applied field.

Acknowledgments

We would like to thank F Tasset, E Lelievre Berna and E Bourgeat-Lami for their efforts in setting up Cryopad II.

References

[1] Sechovsky V and Havela L 1988 *Ferromagnetic Materials* vol 4, ed K H J Buschow (Amsterdam: North-Holland) p 309
[2] Fournier J-M and Troć R 1985 *Handbook on Physics and Chemistry of the Actinides* vol 29, ed A J Freeman and G H Lander (Amsterdam: North-Holland) p 29
[3] Ott H R, Felder E, Schilling A, Dommann A and Hulliger F 1989 *Solid State Commun.* **71** 549
[4] Kontani M, Nishioka T, Hamaguchi Y, Ogura Y, Matsui H, Sato N and Adachi K 1990 *J. Magn. Magn. Mater.* **90/91** 456
[5] Trovalrelli O, Stickar P, Serene J G, Schmerber G and Kappler J P 1994 *Solid State Commun.* **89** 421
[6] Dommann A and Hullinger F 1988 *J. Less-Common Met.* **141** 261
[7] Dommann A, Ott H R, Hullinger F and Fischer P 1990 *J. Less-Common Met.* **160** 171
[8] Smith J G, Bi Y J, Crangle J, Neumann K-U, Zayer N and Ziebeck K R A 1995 *J Magn. Magn. Mater.* **140–144** 1375
[9] Arrott A 1957 *Phys. Rev.* **108** 1394
[10] Zeyen C M E, Chagnon R, Disdier F and Morin H 1984 *Rev. Phys. Appl.* **19** 789
[11] Stassis C 1970 *Phys. Rev. Lett.* **24** 1415
[12] Shull C G 1962 *Phys. Rev. Lett.* **10** 297
[13] Lebech B, Wulff M and Lander G H 1991 *J. Appl. Phys.* **69** 5891
[14] Desclaux J P and Freeman A J 1978 *J. Magn. Magn. Mater.* **8** 119
[15] Papoular R and Gillon B 1990 *Europhys. Lett.* **13** 429
[16] Paixão J A, Lander G H, Brown P J, Nakotte H, de Boer F R and E Brúck 1992 *J. Phys.: Condens. Matter* **4** 829
[17] Nunez V, Brown P J, Forsyth J B and Tasset F 1991 *Physica* B **174** 60
[18] Brown P J 1993 *Physica* B **192** 14
[19] Brown P J, Forsyth J B and Tasset F 1993 *Proc. R. Soc.* A **442** 147
[20] Brown P J, Nunez V, Tasset F, Forsyth J B and Radhakrishna P 1990 *J. Phys.: Condens. Matter* **2** 9409